International Journal of Thermophysics (2023) 44:90
https://doi.org/10.1007/s10765-023-03198-y

# Speed of Sound in Gaseous 1,1-Difluoroethene (R1132a) at Temperatures Between 193 K and 383 K at Pressures up to 3 MPa

**Defne Demirdesen[1] · Carsten Wedler[1] · Robert E. Low[2] · J. P. Martin Trusler[1]**

Received: 1 March 2023 / Accepted: 29 March 2023


**Abstract**
The speed of sound in gaseous 1,1-difluoroethene (refrigerant R1132a) was measured at temperatures between 193 K and 383 K at pressures up to the lesser of approximately 85 % of the vapour pressure and 3 MPa. The measurements were carried out using a bespoke cylindrical acoustic resonator. The acoustic path length of the resonator was calibrated as a function of temperature by measuring resonance frequencies of the cavity filled with nitrogen gas. The measurements on nitrogen also served to validate the measurement system. The expanded relative uncertainty of the speed of sound in 1,1-difluoroethene at 95% probability was estimated to be 0.021 %. Comparing the results with a preliminary equation of state for 1,1-difluoroethene shows deviations within $\pm 0.3$ %.

**Keywords** 1,1-Difluoroethene · R1132a · Sound speed

## 1 Introduction

1,1-Difluoroethene has been identified as a possible component of refrigerant fluids for ultra-low-temperature applications. Thermophysical properties of the fluid are an important consideration and, to date, a limited suite of experimental measurements have been reported. These include saturation properties [1–3], liquid- and vapour-phase $pVT$ properties [3–5], surface tension, liquid and vapour viscosity and liquid thermal conductivity [5]. A preliminary Helmholtz-energy-explicit equation of state has been proposed to describe the thermodynamic properties of this fluid [5].

Special Issue in Honor of Professor Roland Span's 60th Birthday.

✉ J. P. Martin Trusler
m.trusler@imperial.ac.uk

[1] Department of Chemical Engineering, Imperial College London, South Kensington Campus, London SW7 2AZ, UK

[2] Koura Global R&D, The Heath Business & Technical Park, Runcorn WA7 4QX, UK

Published online: 24 April 2023

This Helmholtz equation of state is in the form of the 12-term fundamental equation for polar components proposed by Span in his seminal book *Multiparameter Equations of State: An Accurate Source of Thermodynamic Property Data* [6] and a series of articles by Span and Wagner [7–9]. For several polar refrigerant fluids such as fluoromethane, 1-chloro-1,1-difluoroethane, and 1,1-dichloro-1-fluoroethane, the 12-term fundamental equations developed by Lemmon and Span [10] are state-of-the-art and recommended by NIST [11]. The objective of the present work was to extend the available data by contributing measurements of the speed of sound in the gas phase over an extended range of temperatures and to validate the preliminary 12-term fundamental equation for 1,1-difluoroethene.

## 2 Experimental

### 2.1 Samples

Table 1 details the source and purity of the chemical used in this work. Approximately 0.5 kg of the 1,1-difluoroethene was supplied as liquefied gas in a 0.5 L stainless-steel sample vessel. An analysis of the sample by gas chromatography gave a purity of 99.97 mol% and the principal uncertainty was identified as 1-fluoroethene.

### 2.2 Apparatus

The speed of sound was measured with a cylindrical acoustic resonator based on the design of Ruffine and Trusler [12]. The resonator, shown in Fig. 1, comprised a stainless-steel (AISI type 316L) cylindrical cavity of 60 mm nominal length, 15 mm internal diameter and 24 mm external diameter, closed at each end by piezoelectric transducer assemblies. The transducers were fabricated from cylinders of stainless steel, 24 mm in diameter and 10 mm long, counter-bored to create a flat diaphragm of thickness 0.8 mm and diameter 15 mm. The transducers, cover plates and the body of the cylinder were bolted together such that the diaphragms approximated edge-clamped circulate plates.

In the centre of each diaphragm, external to the cylindrical cavity resonator, a circular recess of 0.2 mm depth and 10.2 mm diameter accommodated a 10 mm diameter × 0.4 mm thick piezoelectric ceramic disc (Piezo Technologies Inc., type K350)

**Table 1** Description of materials used, where $x$ denotes mole fraction

| Chemical name | CAS Number | Source | Purity as supplied | Additional purification |
|---|---|---|---|---|
| Nitrogen | 7727-37-9 | BOC | $x \geq 0.99995$ | None |
| 1,1-difluoroethene (R1132a) | 75-38-7 | Koura Business Group | $x = 0.9997$[a] | None |

[a]Supplier's GC analysis

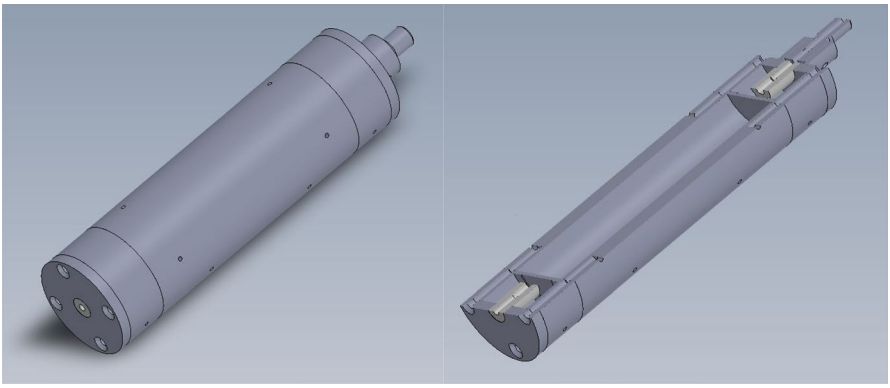

**Fig. 1** Cylindrical acoustic resonator

which was bonded in place with a thin film of epoxy resin (Loctite Stycast FT2850 with catalyst 23LV). The piezoelectric discs were provided with fired-on gold electrodes on both faces. During bonding, pressure was applied to the joint such that electrical contact was established between the face of the disc and the diaphragm through the epoxy layer, exploiting the concentric tooling marks on the metal. Since, in the final assembly, the resonator was grounded, this provided one common electrical connection to the two transducers. The other connection to each transducer was provided by a spring contact, mounted on a PEEK insulator inserted into the cover plate (see Fig. 1), to which a length of PTFE-insulated wire was soldered. The wires from each transducer exited from the pressure vessel through hermetically sealed feedthroughs terminating in female BNC connectors.

Eight holes of 1 mm diameter were drilled through the wall of the cylinder to allow gas to enter and leave the cavity. Four such holes were located 90° apart at a distance of 15 mm from each end of the cavity. This placement coincided with a node of the standing acoustic pressure wave when the cavity was excited in the resonance mode used to determine the speed of sound, thereby ensuring that the holes had a negligible effect on the measured resonance curve.

The cylindrical resonator was mounted within a cylindrical stainless-steel pressure vessel (Sitec model 740.1361-H2, Type EN 1.4980) sealed with a PTFE-graphite composite o-ring. The pressure vessel was provided with fluid ports at both ends. The port at the top of the vessel was used both for gas inlet/outlet and as a conduit for one transducer wire. The port at the bottom of the vessel was used only as a conduit for the other transducer wire. The vessel was immersed in a refrigerated thermostatic bath (Fluke model 7381) filled with 3-ethoxy-1,1,1,2,3,4,4,5,5,6,6,6-dodecafluoro-2-trifluoromethyl-hexane (3 M thermal fluid Novec 7500). This bath could be operated at temperatures between 193.15 K and 383.15 K.

As shown in Fig. 2, the inlet port of the pressure vessel was connected via 3.2 mm o.d. stainless-steel tubing to a system of valves and fittings that provided connections for a pressure sensor, nitrogen gas inlet, sample inlet and an outlet line. The latter could be connected via valve V4 either to a vacuum pump or to a 10 L

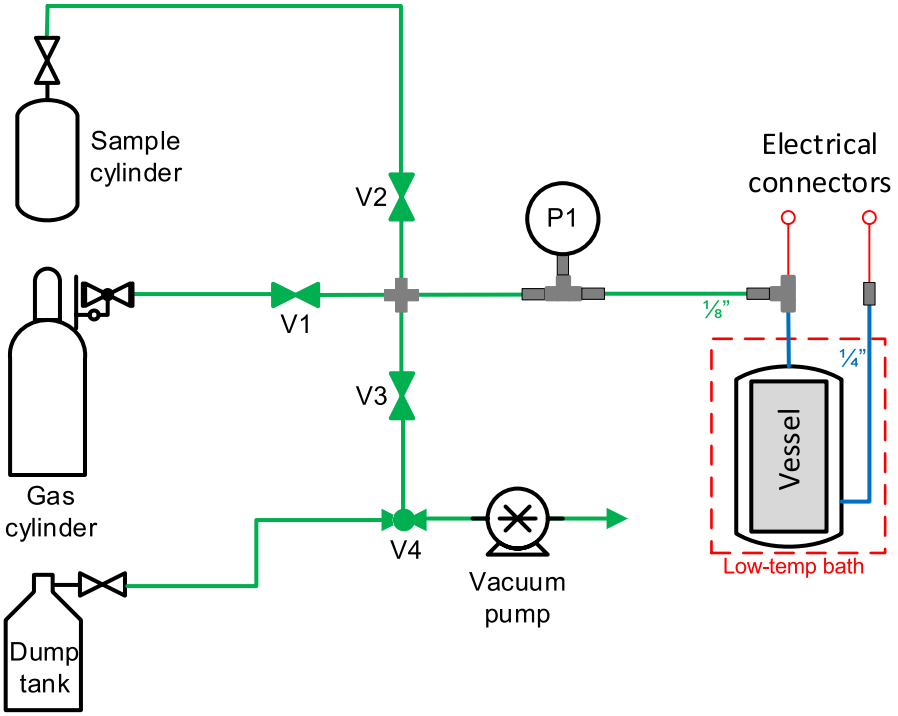


**Fig. 2** Schematic diagram of the measurement system: V1–V4, valves; P1, pressure sensor

aluminium tank. The latter was evacuated at the start of the measurement campaign and subsequently used as a sink into which used 1,1-difluoroethene could be safely transferred without releasing it to the atmosphere.

The pressure was measured with a digital transmitter (P1 in Fig. 2) with a full-scale range of 3 MPa and a standard uncertainty of 0.001 MPa (Keller model PAA-33X). This sensor was calibrated by the supplier. The temperature was measured with an industrial platinum resistance thermometer (PRT) inserted into a thermowell in the wall of the pressure vessel, the resistance of which was measured with a data acquisition unit (Keysight model 34970A). The PRT was calibrated in a triple-point-of-water cell and by comparison in the fluid bath with a standard platinum resistance thermometer at temperatures between 203.15 K and 373.15 K. The overall standard uncertainty of the measured temperature was estimated to be 0.02 K.

A function generator (Agilent model 33210A) was used to drive the source transducer with a sine wave voltage of peak-to-peak amplitude 20 V. To measure a resonance frequency of the gas-filled cavity, the driving frequency was stepped through a sequence of evenly spaced values over a range of $\pm$ two half widths centred approximately on the resonance frequency. The amplitude and phase of the received signal was measured at each frequency with a lock-in amplifier (Stanford Research Systems SRS830) and the resulting data were analysed in a standard way [13] to determine the precise resonance frequency with a fractional repeatability of better than $1 \times 10^{-5}$.

## 3 Acoustic Model

As in the work of Ruffine and Trusler [12], we make use of just one resonant mode of the gas-filled cylindrical cavity: the second longitudinal mode. The rational for this is as follows: first, all the odd-order longitudinal modes couple to vibration of the cylinder body so that only even-order modes should be used; second, the measurement should be carried out at frequencies well below the resonance frequency of the plate transducers; third, the resonator diameter should be small to limit the size of the required pressure vessel, thereby eliminating low-frequency radial modes; fourth, the holes through which gas is admitted should coincide with nodal planes of the resonant mode(s) employed. These requirements essentially restrict operation to the second longitudinal mode.

The resonance frequency $f_{200}$ of the second longitudinal mode is given by

$$f_{200} = (c/L) + \Delta f, \tag{1}$$

where $L$ is the length of the cavity, $c$ is the thermodynamic speed of sound, and $\Delta f$ is the sum of three small correction terms [12, 14]:

$$\Delta f = 2\Delta f_{\mathrm{end}} + \Delta f_{\mathrm{v-t}} + \Delta f_{\mathrm{vib}}. \tag{2}$$

Here, $\Delta f_{\mathrm{end}}$ accounts for the non-rigid condition on the face of one transducer, $\Delta f_{\mathrm{v-t}}$ accounts for the visco-thermal boundary layers at the walls of the cavity, and $\Delta f_{\mathrm{vib}}$ accounts for any vibrational relaxation effects that cause the speed of sound at the measurement frequency to differ from that at zero frequency.

The end-plate correction is given by

$$\Delta f_{\mathrm{end}} = \frac{-\rho c^2 (C/L) f_{200}}{1 - (f_{200}/f_1)^2}, \tag{3}$$

where $\rho$ is the gas density, $C$ is the static compliance (averaged over the face) and $f_1$ is the fundamental resonance frequency of the end plate. For a homogeneous untensioned edge-clamped circular plate of radius $b$ and thickness $d$, these quantities are given by [14, 15]

$$C = \frac{(1-\sigma^2) b^4}{16 E d^3}, \tag{4}$$

$$f_1 = \nu_1^2 \left( \frac{d}{4\pi b^2} \right) \sqrt{\frac{E}{3\rho_{\mathrm{s}}(1-\sigma^2)}}, \tag{5}$$

where $\nu_1 = 1.015\pi$, $E$ is Young's modulus, $\sigma$ is Poisson's ratio and $\rho_{\mathrm{s}}$ is the density of the diaphragm material. However, the actual diaphragm differs from this ideal and, consequently, $f_1$ in Eq. 3 was determined experimentally while $C$ was treated as a calibration parameter. This correction was always less than 0.06% of the measured resonance frequency.

The visco-thermal boundary-layer correction is given by [12, 14]

$$\Delta f_{\mathrm{v-t}} = -\tfrac{1}{2} f_{200}\left[(1+2b/L)(\gamma-1)D_{\mathrm{t}}^{1/2} + D_{\mathrm{v}}^{1/2}\right] \Big/ \sqrt{\pi f_{200} b^2}, \tag{6}$$

where $D_{\mathrm{t}} = \lambda/(\rho c_p)$ is the thermal diffusivity, $D_{\mathrm{v}} = \eta/\rho$ is the viscous diffusivity, $\lambda$ is the thermal conductivity, $c_p$ is the isobaric specific heat capacity, and $\eta$ is the shear viscosity. Additionally, $\gamma$ is the ratio of the specific heat capacity at constant pressure to that at constant volume. This correction was always less than 0.15 % of the measured resonance frequency.

The vibrational correction was assumed to be negligible for the test gas. This is justified because vibrational relaxation times in polyatomic molecules are typically very short in comparison with the period of the sound waves used in this work. In the few cases, such as carbon dioxide, where this is not the case high sound absorption is observed whereas, in this work, this was not the case; this is discussed further in Sect. 4.3. However, for the calibration with nitrogen, the situation was different and the following correction was used:

$$\Delta f_{\mathrm{vib}} = f_{200}\left[\sqrt{\frac{\gamma(c_p - c_{\mathrm{vib}})}{(c_V - c_{\mathrm{vib}})}} - 1\right], \tag{7}$$

where $c_{\mathrm{vib}}$ is the vibrational contribution to the heat capacity which was calculated from a Planck-Einstein function with a vibrational characteristic temperature 3395 K [16]. This correction reflects the very long vibrational relaxation time of the nitrogen molecule, which causes the vibrational mode to be 'frozen' on the time scale of the acoustic cycle. Since $c_{\mathrm{vib}} < 0.01R$ at the temperatures in question, the magnitude of the relative correction is < 0.06 % and the associated uncertainty is negligible. Of course, this correction could have been avoided entirely by calibrating with a monatomic gas such as argon.

### 3.1 Thermophysical Properties

Implementation of the acoustic model requires approximate values of the following thermophysical properties of the gas under study: density, isobaric specific heat capacity, isochoric specific heat capacity, speed of sound, thermal conductivity and viscosity. In the case of nitrogen, we employed the equation of state of Span et al. [17] and the transport-property correlations reported by Lemmon and Jacobsen [18]. The relative uncertainties of the viscosity and thermal conductivity of nitrogen are given as 0.5 % and 2 %, respectively, while the uncertainties of the thermodynamic properties are negligible in the context of the small corrections required.

For 1,1-difluoroethene, we use the preliminary equation of state of Low [5] to obtain $\rho$, $c_p$, $\gamma$ and $c$. The dilute-gas viscosity of 1,1-difluoroethene has been measured at temperature of between approximately 223 K and 421 K [5]. The experimental viscosity data are plotted as a function temperature in Fig. 3 and can be correlated precisely as a linear function of temperature as follows:

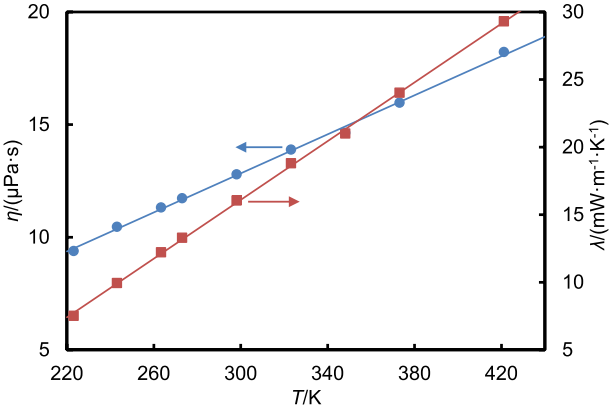


**Fig. 3** Experimental viscosity $\eta$ [5] (●) and predicted thermal conductivity $\lambda$ (■) of 1,1-difluoroethene as a dilute gas as a function of temperature $T$

$$\eta/(\mu\text{Pa}\cdot\text{s}) = -0.164 + 0.04333(T/\text{K}). \tag{8}$$

Since no thermal conductivity data were available, we estimated this quantity based on the experimental viscosity and the Prandtl number $P_r = \eta c_p/\lambda$ of 1,1-difluoroethane (R152a), a molecule with a similar size, mass and dipole moment. Values of $P_r$ were calculated using the REFPROP version 10 software [19] based on the viscosity correlation of Klein et al. [20] and the thermal conductivity model of Krauss [21] together with the equation of state of Outcalt and McLinden [22]. The predicted thermal conductivities of 1,1-difluoroethene are plotted in Fig. 3 and can be represented by the following linear equation:

$$\lambda/(\text{mW}\cdot\text{m}^{-1}\cdot\text{K}^{-1}) = -16.49 + 0.10865(T/\text{K}). \tag{9}$$

The pressure dependences of the viscosity and thermal conductivity were neglected. Unfortunately, the uncertainty of the experimental gas viscosity data for 1,1-difluoroethene was not specified. For purposes of uncertainty analysis, we assumed a relative uncertainty of 5 % for viscosity and 10 % for thermal conductivity. Plausible uncertainties in the thermodynamic properties have a negligible influence on the calculated corrections.

## 4 Results

### 4.1 Calibration and Verification Measurements

The path length $L$ of the resonator was determined as a function of temperature, along with the end-plate compliance $C$ and resonance frequency $f_1$ (both assumed constant) in calibration measurements. The resonance frequency of the plate

transducer predicted using Eq. 5 with handbook values for the elastic constants of type 316L stainless steel is approximately 36 kHz. To determine $f_1$ experimentally, the two transducers where attached to either end of a short cylindrical coupler of length 6 mm and the spectrum was recorded in ambient air. The largest peak in the received amplitude was observed at 26.5 kHz and this was taken as the resonance frequency with an estimated standard uncertainty of 0.5 kHz. This frequency is below the lowest longitudinal resonance frequency of the short cylindrical cavity.

The remainder of the calibration was accomplished by measuring the resonance frequency $f_{200}$ in nitrogen gas along a set of five isotherms with pressures up to 3 MPa. Initially, each isotherm was analysed separately to determine values of the path length $L$ and the end-plate compliance $C$ by linear regression according to the relation:

$$\frac{c}{(f_{200} - \Delta f_{\mathrm{v-t}} - \Delta f_{\mathrm{vib}})} = L + C\left[\frac{2\rho c^2}{1 - (f_{200}/f_1)^2}\right]. \tag{10}$$

This equation was derived by combining Eqs. 1, 2 and 3, neglecting second-order correction terms. Since $\rho c^2 \approx \gamma p$, the right hand side is approximately proportional to pressure. The speed of sound and other thermophysical properties of nitrogen were calculated from the models of Span et al. [17] and Lemmon and Jacobsen [18] as discussed above. Figure 4 illustrates the analysis for the isotherm at $T = 273.31$ K.

Repeating the analysis at each temperature, it was observed that the path length could be correlated with the simple equation

$$\ln(L/L_0) = \alpha_0 t + \tfrac{1}{2}\alpha_1 t^2, \tag{11}$$

where $t = (T - 273.15\ \mathrm{K})$. The values obtained for the parameters in Eq. 11 were $L_0 = 60.00291$ mm, $\alpha_0 = 15.233 \times 10^{-6}$ K$^{-1}$ and $\alpha_1 = 9.78 \times 10^{-9}$ K$^{-2}$. According

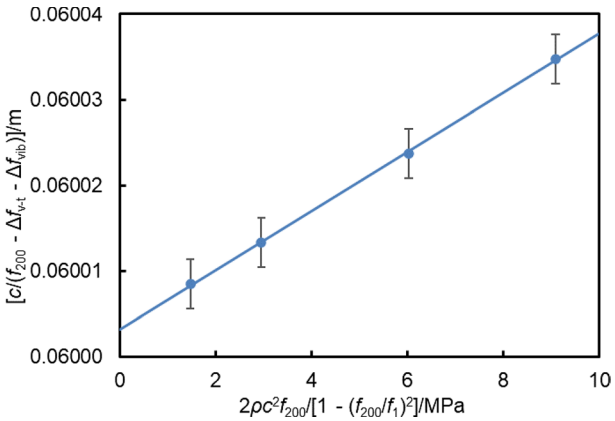


**Fig. 4** Calibration data measured in nitrogen at $T = 273.31$ K where $c$ is calculated speed of sound, $\rho$ is calculated density, $f_{200}$ is the experimental second longitudinal resonance frequency, $f_1$ is the transducer plate resonance frequency, and $\Delta f_{\mathrm{v-t}}$ and $\Delta f_{\mathrm{vib}}$ are calculated visco-thermal and vibrational corrections: ●, experiment; ———, Eq. (10)

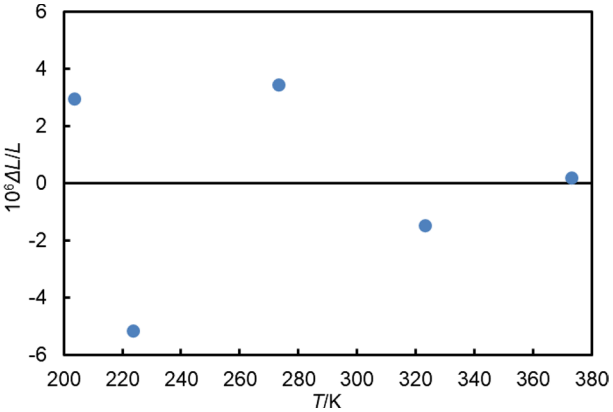


**Fig. 5** Relative deviation $\Delta L/L$ of pathlengths determined at each temperature $T$ from Eq. 11: ●, isothermal values; ———, Eq. 11. Error bars are too large to plot at this scale

**Table 2** Uncertainty budget for determination of the path length $L$ from measurements in nitrogen along the isotherm at $T=273.31$ K, where $f_{200}$ is the second longitudinal resonance frequency, $T$ is temperature, $p$ is pressure, $\eta$ is viscosity, $\lambda$ is thermal conductivity, $f_1$ is end-plate resonance frequency, and $c$ is speed of sound

| Quantity | Value or range | Standard uncertainty | Sensitivity factor | Standard uncertainty |
|---|---|---|---|---|
| $f_{200}$ | (5617 to 5682) Hz | 0.01 Hz | $1.1\times10^{-5}$ m·Hz$^{-1}$ | 0.000 000 1 m |
| $T$ | 273.31 K | 0.02 K | $1.1\times10^{-4}$ m·K$^{-1}$ | 0.000 002 2 m |
| $p$ | $(0.5 \text{ to } 3.0)\times10^6$ Pa | 1000 Pa | $2.5\times10^{-4}$ m·Pa$^{-1}$ | 0.000 000 2 m |
| $\eta$ | $(1.67 \text{ to } 1.71)\times10^{-6}$ Pa·s | $8.5\times10^{-8}$ Pa·s | $2.5\times10^{-5}$ m·Pa$^{-1}$·s$^{-1}$ | 0.000 000 1 m |
| $\lambda$ | $(24.2 \text{ to } 25.4)\times10^{-3}$ W·m$^{-1}$·K$^{-1}$ | $4.9\times10^{-4}$ W·m$^{-1}$·K$^{-1}$ | $1.5\times10^{-5}$ m$^2$·K·W$^{-1}$ | 0.000 000 3 m |
| $f_1$ | 26,500 Hz | 500 Hz | $7.5\times10^{-13}$ m·Hz$^{-1}$ | 0.000 000 0 m |
| $c$ | (337.5 to 341.3) m·s$^{-1}$ | 0.010 m·s$^{-1}$ | $1.8\times10^{-4}$ s | 0.000 001 8 m |
| $L$ | 0.060033 m | $1.4\times10^{-7}$ m[a] | 1 | 0.000 000 1 m |
| | | Overall standard uncertainty: | | 0.000 002 9 m |

[a]Standard uncertainty from regression analysis

to Eq. 11, the linear expansivity is $\alpha_0+\alpha_1 t$ which varies from $14.6\times10^{-6}$ K$^{-1}$ at 203.15 K to $16.2\times10^{-6}$ K$^{-1}$ at 373.15 K. Figure 5 shows the relative deviations of the path length from Eq. 11 and these are observed to be within $\pm6\times10^{-6}$, about one order of magnitude smaller than the estimated standard uncertainty of the data. This indicated that the path lengths obtained are much smoother than their overall uncertainty.

The uncertainty budget for the determination of $L$ at $T=273.31$ K is detailed in Table 2 and includes contributions from all quantities appearing explicitly or implicitly in the calibration equation, Eq. 10. The last item for $L$ itself is the standard error of the intercept determined in the linear regression with Eq. 10 and accounts for all

random effects along the isotherm. The overall relative standard uncertainty of $L$ is 0.0048 %. The much smaller relative deviations from Eq. 11 indicate that the correlation of $L$ as a function of $T$ contributed negligible additional uncertainty.

As shown in Fig. 6, the mean compliance of the end plate $C$ obtained from the slope of the regression line with Eq. 10 could be represented as a linear function of temperature:

$$C = C_0 + C_1 t. \tag{12}$$

The coefficients in Eq. 12 are $C_0 = 3.488$ m·TPa$^{-1}$ and $C_1 = 0.00393$ m·TPa$^{-1}$·K$^{-1}$, and the values of $C$ are approximately twice that given by Eq. 4. The standard relative uncertainty of $C$ on an isotherm, determined by regression analysis, about 1% and, as shown in Fig. 6, the values correlate as a linear function of temperature approximately within the uncertainty. For the purposes of error propagation, the standard relative uncertainty of this term was inflated to 5%.

With use of calibration Eqs. 11 and 12, the speed of sound obtained in nitrogen are in very close agreement with the equation of state of Span et al. [17] along the five isotherms investigated. As shown in Fig. 7, all fall within ± 0.003 % which is well within the standard relative uncertainty of the equation of state of about 0.005%. Given that 19 experimental data points were reconciled with 5 adjustable calibration parameters ($L_0$, $a_0$, $a_1$, $C_0$, and $C_1$), these results also serve as a validation of the instrument.

### 4.2 Speed of Sound in 1,1-Difluoroethene

The speed of sound was measured in 1,1-difluoroethene along nine isotherms with pressures up to the lower of approximately 85 % of the vapour pressure and 3 MPa. Measurements were not made closer to the saturation line so as to avoid systematic

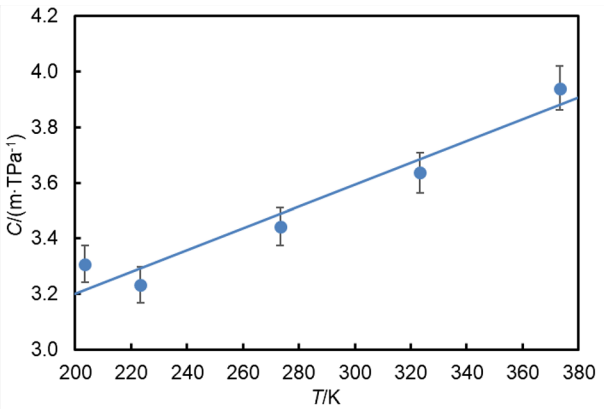


**Fig. 6** Mean end-plate compliance $C$ as a function of temperature $T$: ●, experiment; ———, Eq. 12. Error bars represent the standard uncertainty of the slope from regression with Eq. 10

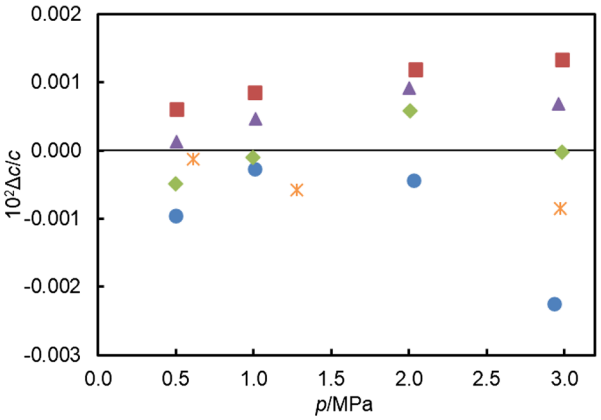


**Fig. 7** Deviation $\Delta c = c - c_{EoS}$ between experimental speed of sound $c$ in nitrogen and values $c_{exp}$ calculated from the equation of state of Span and Lemmon [17] as a function of pressure $p$ along isotherms: ●, $T = 203.52$ K; ■, $T = 223.41$ K; ◆, $T = 273.31$ K; ▲, $T = 323.26$ K; ✳, $T = 373.23$ K. Error bars are too large to show at this scale

errors arising from pre-condensation on the walls of the cavity [23]. At $T \leq 323.3$ K, the lowest pressure on each isotherm was generally about 0.1 MPa, except at 223 K where measurements went down to 0.05 MPa. Lower pressures were not measured because the acoustic signals diminished very rapidly with reducing pressure. Furthermore, at temperatures above the glass transition temperature of the epoxy resin (approximately 340 K), the efficiency of the transducers was substantially reduced, limiting operation to pressures above about 0.5 MPa.

Table 3 details the uncertainty budget for the speed of sound in 1,1-difluoroethene, evaluated at an exemplary state point. The expanded relative uncertainty at 95% confidence ($k = 2$) is 0.021 %. Individual terms in the uncertainty budget vary

**Table 3** Uncertainty budget for speed of sound $c$ in 1,1-difluoroethene at $T = 298.29$ K and $p = 1.4995$ MPa, where $f_{200}$ is the second longitudinal resonance frequency, $T$ is temperature, $p$ is pressure, $\eta$ is viscosity, $\lambda$ is thermal conductivity, $f_1$ is end-plate resonance frequency, $C$ is mean end-plate compliance, and $L$ is path length

| Quantity | Value | Standard uncertainty | Sensitivity factor | Standard uncertainty |
|---|---|---|---|---|
| $f_{200}$ | 3213.45 Hz | 0.01 Hz | 0.0600 m | 0.0006 $m \cdot s^{-1}$ |
| $T$ | 298.29 K | 0.02 K | 0.535 $m \cdot s^{-1} \cdot K^{-1}$ | 0.0107 $m \cdot s^{-1}$ |
| $p$ | $1.4995 \times 10^6$ Pa | 1000 Pa | $14.4 \times 10^{-6}$ $m \cdot s^{-1} \cdot Pa^{-1}$ | 0.0144 $m \cdot s^{-1}$ |
| $\eta$ | $12.8 \times 10^{-6}$ Pa·s | $0.64 \times 10^{-6}$ Pa·s | $2.66 \times 10^3$ $m \cdot s^{-2} \cdot Pa^{-1}$ | 0.0017 $m \cdot s^{-1}$ |
| $\lambda$ | $15.9 \times 10^{-3}$ $W \cdot m^{-1} \cdot K^{-1}$ | $1.59 \times 10^{-3}$ $W \cdot m^{-1} \cdot K^{-1}$ | 0.808 $m^2 \cdot s^{-1} \cdot K \cdot W^{-1}$ | 0.0013 $m \cdot s^{-1}$ |
| $f_1$ | 26,500 Hz | 1000 Hz | $3.43 \times 10^{-8}$ m | 0.0000 $m \cdot s^{-1}$ |
| $C$ | $3.59 \times 10^{-12}$ $m \cdot Pa^{-1}$ | $0.18 \times 10^{-12}$ $m \cdot Pa^{-1}$ | $1.93 \times 10^{-2}$ $Pa \cdot s^{-1}$ | 0.0019 $m \cdot s^{-1}$ |
| $L$ | 0.060 026 m | 0.000 002 9 m | 3215 $s^{-1}$ | 0.0093 $m \cdot s^{-1}$ |
| | | Overall expanded uncertainty ($k = 2$): | | 0.041 $m \cdot s^{-1}$ |

with state point but the overall relative uncertainty (dominated by the uncertainties of $T$, $p$ and $L$) is approximately constant and we therefore ascribe the same relative uncertainty at the median state point to all states.

Table 4 lists the experimental speeds of sound. In Fig. 8, we plot the results against pressure along each isotherms in comparison with the predictions of the preliminary equation of state [5]. Remarkable, all of the results fall within $\pm 0.3$ % of the equation of state. There is a clear trend of slight positive deviations from the equation of state at low pressures and low temperatures, suggesting that the current

**Table 4** Speeds of sound $c$ in 1,1-difluoroethene at temperatures $T$ and pressures $p$

| $T$/K | $p$/MPa | $c$/(m·s$^{-1}$) | $T$/K | $p$/MPa | $c$/(m·s$^{-1}$) |
|---|---|---|---|---|---|
| 193.492 | 0.1014 | 172.314 | 273.317 | 0.1012 | 203.377 |
| 203.517 | 0.1818 | 174.021 | 298.293 | 2.9431 | 168.278 |
| 203.516 | 0.1496 | 175.202 | 298.293 | 2.5041 | 176.684 |
| 203.516 | 0.1205 | 176.237 | 298.292 | 1.9984 | 185.313 |
| 203.517 | 0.0902 | 177.373 | 298.292 | 1.4994 | 193.025 |
| | | | 298.292 | 0.9973 | 200.163 |
| 223.421 | 0.4016 | 176.383 | 298.292 | 0.5072 | 206.663 |
| 223.422 | 0.3007 | 179.486 | 298.292 | 0.1036 | 211.713 |
| 223.424 | 0.2476 | 181.050 | | | |
| 223.422 | 0.2023 | 182.360 | 323.270 | 2.9978 | 188.270 |
| 223.420 | 0.1509 | 183.796 | 323.266 | 2.5080 | 194.068 |
| 223.420 | 0.1009 | 185.171 | 323.269 | 1.9973 | 199.900 |
| 223.423 | 0.0507 | 186.561 | 323.268 | 1.4909 | 205.461 |
| | | | 323.268 | 1.0019 | 210.629 |
| 243.371 | 0.8331 | 174.688 | 323.259 | 0.5057 | 215.663 |
| 243.372 | 0.7017 | 178.377 | 323.260 | 0.1046 | 219.545 |
| 243.375 | 0.6049 | 180.937 | | | |
| 243.373 | 0.4972 | 183.649 | 373.234 | 3.0348 | 216.352 |
| 243.372 | 0.4008 | 185.983 | 373.233 | 2.5008 | 219.645 |
| 243.372 | 0.3004 | 188.320 | 373.233 | 2.0186 | 222.668 |
| 243.373 | 0.2023 | 190.559 | 373.233 | 1.5106 | 225.885 |
| 243.374 | 0.0986 | 192.834 | 373.235 | 1.0059 | 229.137 |
| | | | 373.236 | 0.5045 | 232.138 |
| 273.316 | 2.0068 | 165.227 | | | |
| 273.315 | 1.7268 | 172.542 | 383.222 | 3.0135 | 220.925 |
| 273.315 | 1.5156 | 177.464 | 383.223 | 2.4549 | 224.001 |
| 273.316 | 1.2530 | 183.060 | 383.221 | 1.9892 | 226.619 |
| 273.316 | 1.0167 | 187.714 | 383.223 | 1.4962 | 229.434 |
| 273.316 | 0.7210 | 193.128 | 383.221 | 0.9858 | 232.364 |
| 273.315 | 0.5169 | 196.648 | 383.221 | 0.5105 | 235.267 |
| 273.314 | 0.2612 | 200.847 | | | |

Standard uncertainties are $u(T) = 0.02$ K, $u(p) = 0.001$ MPa and $u(c)/c = 0.011$ %

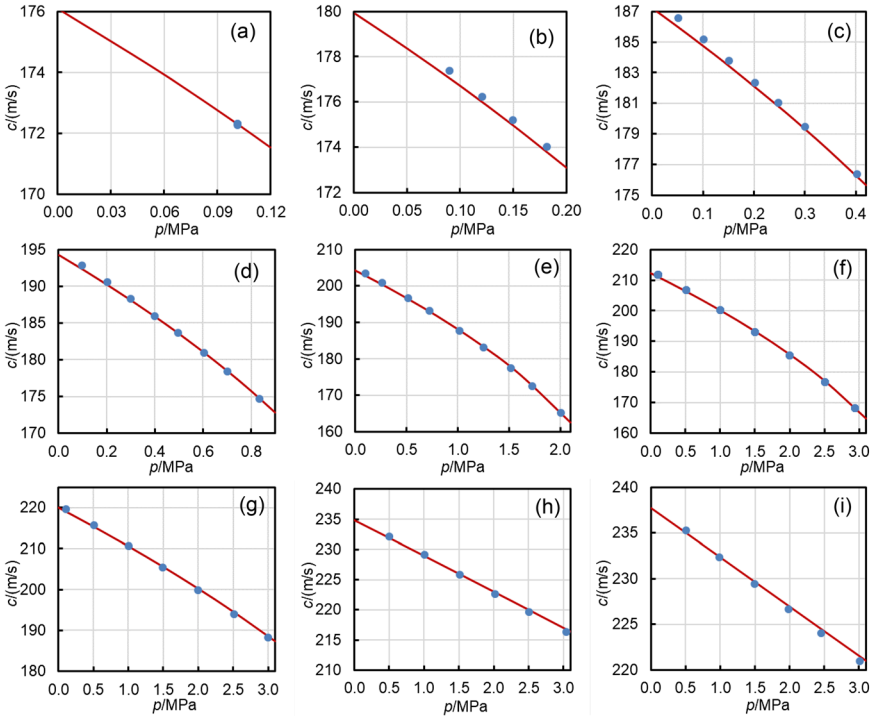


**Fig. 8** Speeds of sound $c$ in 1,1-difluoroethene as function of pressure $p$ along isotherms at temperatures $T$: (a) $T=193.49$ K; (b) $T=203.52$ K; (c) $T=223.42$ K; (d) $T=243.37$ K; (e) $T=273.32$ K; (f) $T=298.29$ K; (g) $T=323.27$ K; (h) $T=373.23$ K; (i) $T=383.22$ K. ●, this work; ———, calculated from the preliminary equation of state [5]

model slightly over estimates the ideal-gas isobaric specific heat capacity at low temperatures.

### 4.3 Resonance Half Widths

According to the acoustic model, the half width $g$ of a resonance mode of the gas-filled cavity is the sum of boundary-layer and bulk sound absorption terms. The former is the negative of $\Delta f_{\text{v-t}}$ and the latter generally comprises visco-thermal and relaxation contributions:

$$g = -\Delta f_{\text{v}} - \text{t} + (\pi f^2 / c^2)\left[\tfrac{4}{3}D_{\text{v}} + (\gamma - 1)D_{\text{t}} + \eta_{\text{b}} / \rho\right]. \tag{13}$$

Here, $\eta_{\text{b}}$ is a bulk viscosity associated with molecular thermal relaxation. In the present case, $\eta_{\text{b}}$ is negligible for nitrogen on account of the vibrational relaxation time being much longer than the period of the sound wave [16]. For 1,1-difluoroethene, $\eta_{\text{b}}$ is unknown but, if significant, might be estimated by comparing the experimental half widths with Eq. 13. For both gases, the bulk visco-thermal terms contribute less than

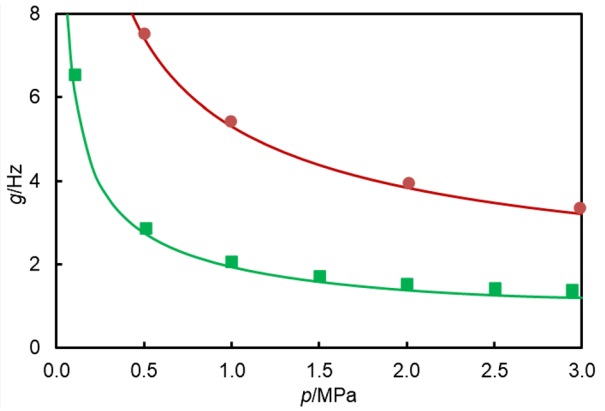


**Fig. 9** Resonance half widths $g$ as a function of pressure $p$: ●, nitrogen at $T = 273.31$ K; ■, 1,1-difluoroethene at $T = 298.29$ K; ———, calculated from Eq. 13

0.01 Hz to the half widths and are negligible in comparison with the boundary-layer term. Figure 9 compares the experimental half widths in both gases with the theoretical values obtained from Eq. 13. For nitrogen, we observe small excess half widths $\Delta g$ of between (0.1 and 0.2) Hz, indicating that dissipation in the real system slightly exceeds the predictions of the model. For 1,1-difluoroethene, $\Delta g$ varies between (0.1 and 0.5) Hz and tend to increase as the pressures decreases. The fact that the excess half widths remain small in 1,1-difluoroethene indicates that dispersion is negligible in this gas. In relative terms, the ratio $\Delta g/f_{200}$ is < 0.003 % for nitrogen and < 0.02 % for 1,1-difluoroethene. These observations provide further validation of the acoustic model and, in particular, of the visco-thermal boundary-layer correction.

## 5 Conclusions

The sound-speed sensor used in this work has been calibrated and validated in an extended range of temperatures (193 K to 383 K) at pressures up to 3 MPa. In this domain, it can be used to obtain speeds of sound with low relative uncertainties on the order of 0.02%. Measurements on a high-purity sample of 1,1-difluoroethene demonstrate that the preliminary equation of state for this substance [5] is substantially correct in the region investigated. The small deviations observed between the experimental data and the equation of state are attributable in significant measure to the ideal-gas heat capacity model. A future adjustment of the equation of state may reconcile these small differences.

**Author Contributions** DD designed and assembled parts of the apparatus and carried out measurements. CW assisted with assembly and testing of the apparatus, and data analysis. REL provided the sample and sample analysis and provided data for use in the data analysis. JPMT supervised the work, carried out measurements and data analysis and drafted the manuscript. All authors reviewed the manuscript.

**Funding** Funding for this work was provide by Koura Global R&D.

**Data Availability** All relevant data are tabulated in the paper.

## Declarations

**Competing interest** The authors declare no competing interests.

**Ethical Approval** Not applicable.



## References

1. W.H. Mears, R.F. Stahl, S.R. Orfeo, R.C. Shair, L.F. Kells, W. Thompson, H. McCann, Ind. Eng. Chem. **47**, 1449 (1955)
2. J. Otto, W. Thomas, Int. J. Heat Mass Transf. **7**, 41 (1964)
3. S. Tomassetti, G. Di Nicola, Fluid Phase Equilib. **533**, 112939 (2021)
4. D.S. Tsiklis, V.M. Prokhorov, Zh. Fiz. Khim. **41**, 2195 (1967)
5. R. Low, In 1st IIR International Conference on the Application of HFO Refrigerants, (IIR, Birmingham, 2018), pp. 13–20
6. R. Span, *Multiparameter Equations of State: An Accurate Source of Thermodynamic Property Data* (Springer, Berlin, 2000)
7. R. Span, W. Wagner, Int. J. Thermophys. **24**, 1 (2003)
8. R. Span, W. Wagner, Int. J. Thermophys. **24**, 41 (2003)
9. R. Span, W. Wagner, Int. J. Thermophys. **24**, 111 (2003)
10. E.W. Lemmon, R. Span, J. Chem. Eng. Data **51**, 785 (2006)
11. M.L. Huber, E.W. Lemmon, I.H. Bell, M.O. McLinden, Ind. Eng. Chem. Res. **61**, 15449 (2022)
12. L. Ruffine, J.P.M. Trusler, Int. J. Thermophys. **30**, 1106 (2009)
13. J.B. Mehl, M.R. Moldover, J. Chem. Phys. **74**, 4062 (1981)
14. J.P.M. Trusler, *Physical Acoustics and Metrology of Fluids* (Adam Higler, Bristol, 1991)
15. J.N. Reddy, *Theory and Analysis of Elastic Plates and Shells*, 2nd edn. (CRC Press, Boca Raton, 2006), p.568
16. M.F. Costa Gomes, J.P.M. Trusler, J. Chem. Thermodyn. **30**, 527 (1998)
17. R. Span, E.W. Lemmon, R.T. Jacobsen, W. Wagner, A. Yokozeki, J. Phys. Chem. Ref. Data **29**, 1361 (2000)
18. E.W. Lemmon, R.T. Jacobsen, Int. J. Thermophys. **25**, 21 (2004)
19. E.W. Lemmon, I.H. Bell, M.L. Huber, M.O. McLinden, (National Institute of Standards and Technology, Gaitherburg, 2018)
20. S.A. Klein, M.O. McLinden, A. Laesecke, Int. J. Refrig **20**, 208 (1997)
21. R. Krauss, V.C. Weiss, T.A. Edison, J.V. Sengers, K. Stephan, Int. J. Thermophys. **17**, 731 (1996)
22. S.L. Outcalt, M.O. McLinden, J. Phys. Chem. Ref. Data **25**, 605 (1996)
23. J.B. Mehl, M.R. Moldover, J. Chem. Phys. **77**, 455 (1982)